Quantitative Analysis of Photochemical Reactions in Pentacene Precursor Films

*Nobutaka Shioya,**,† *Tao Fang,*† *Masamichi Fujii,*† *Ryoi Fujiwara,*† *Hironobu Hayashi,*‡ *Hiroko Yamada,*† *and Takeshi Hasegawa*†

†Institute for Chemical Research, Kyoto University, Gokasho, Uji, Kyoto 611-0011, Japan

‡Center for Basic Research on Materials, National Institute for Materials Science (NIMS), 1-2-1 Sengen, Tsukuba, Ibaraki 305-0047, Japan

Corresponding Author

* To whom correspondence should be addressed.

E-mail: nobutaka@env.kuicr.kyoto-u.ac.jp

ABSTRACT. On-surface reactions are rapidly gaining attention as a chemical technique for synthesizing organic functional materials such as graphene nanoribbons and molecular semiconductors. Quantitative analysis of such reactions is essential for fabricating high-quality film structures, but until our recent work using p-polarized multiple-angle incidence resolution spectrometry (pMAIRS), no analytical technique is available to quantify the reaction rate. In the present study, the pMAIRS technique is employed to analyze the photochemical reaction from 6,13-dihydro-6,13-ethanopentacene-15,16-dione to pentacene in thin films. The spectral analysis on a pMAIRS principle readily reveals the photoconversion rate accurately without other complicated calculations. Thus, this study underlines that the pMAIRS technique is a powerful tool for quantitative analysis of on-surface reactions, as well as molecular orientation.

TOC GRAPHICS

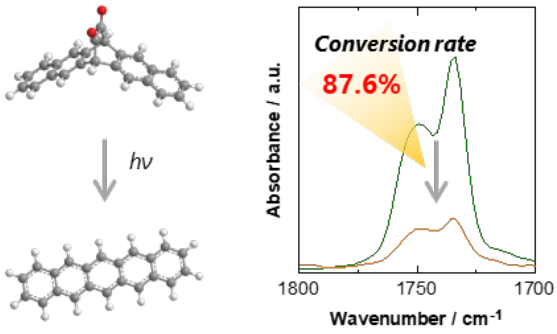

INTRODUCTION

Small-molecule organic semiconductors composed of π-conjugated backbones are used as an active layer in various organic thin-film devices including field-effect transistors (FETs). Solution-processed FETs have recently gained considerable attention due to their large-area electronics and high processability.[1-4] Conventionally used molecular semiconductors for FETs such as pentacene (PEN), however, have low solubility in most solvents, which has been a technical barrier to their use in solution processes. To overcome this barrier, a number of soluble precursors that can chemically be converted to the target substance by heating or photoirradiation have been developed so far.[5–7] In other words, thin films of the target insoluble material can be obtained from the solution-processed precursor thin films by using chemical conversion reactions.

One of the most representative precursors of PEN is 13,6-*N*-sulfinylacetamidopentacene (SAP), and it is thermally converted to the target material,[8,9] as shown in **Figure 1**. This precursor compound is fully converted to PEN by the thermal annealing in thin films, and the converted molecules form a highly ordered polycrystalline structure.[10,11] The precursor compound has an advantage that the desired film is easily obtained, whereas it has a problem that a high annealing temperature of ~420 K or higher is required to complete the thermal conversion.[11] In general, such a high temperature process poses risks of degradation, sublimation, and oxidization for organic semiconductors.

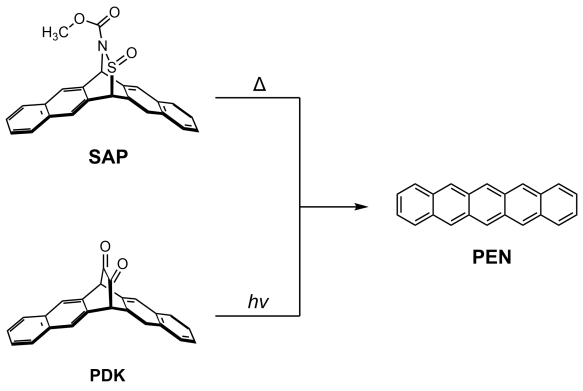

Figure 1. Structural conversion reactions from SAP and PDK to PEN.

As another approach, a photochemically synthetic route to PEN was proposed using 6,13-dihydro-6,13-ethanopentacene-15,16-dione (PDK) as a soluble precursor (**Figure 1**).[12,13] Previous studies reported that the conversion reaction from PDK to PEN proceeds under light irradiation even at room temperature, and that the photoconverted molecules work as a p-type semiconductor in organic thin-film devices.[14–16] In addition, the addition of a high-boiling solvents in the precursor film was reported to be accelerate the conversion reaction and improve the device performance.[14,15] In other words, the conversion rate has a decisive effect on the device performance. They proposed a model in which the additive molecules remain in the precursor film after spin coating to form a semidry film, and the semidry state is essential for promoting the conversion reaction. This model is acceptable considering that solid-state reactions generally require high-thermal energy and a long period of time to proceed.[17–20]

In this manner, the photoconversion reaction from PDK to PEN in thin films is expected for practical applications. Nevertheless, some unresolved matters remain with respect to structural analysis: (1) the residual additives in the model have never been experimentally identified and (2) quantitative analysis of the conversion reaction has not been performed. Infrared (IR) p-polarized multiple-angle incidence resolution spectrometry (pMAIRS)[21,22] is considered best suited for both

purposes. This spectroscopic technique simultaneously provides the in-plane (IP) and out-of-plane (OP) vibrational spectra of an identical thin film with a common ordinate scale, which enables us to perform orientation analysis quantitatively for each chemical group. In addition, an optically isotropic (OI) spectrum that is molecular-orientation free spectrum is also obtained by simply averaging the IP and OP spectra.[11] Since the band intensity of the OI spectrum is proportional only to the quantity of chemical species, the quantitative analysis of chemical reactions can be accurately performed.[11,17,23] IR spectroscopy has another powerful benefit for detecting trace molecules irrespective of the crystallinity,[10] such as impurities including residual solvents.

In the present study, the pMAIRS technique is employed for quantitative analysis of the photoconversion reaction of PDK in spin-coated films. The spectral analysis quantitatively reveals that the conversion reaction is enhanced by adding a high-boiling-point solvent. In addition, the effects of the additive on the film structure in terms of crystallinity and grain size are investigated by using two-dimensional grazing incidence X-ray diffraction (2D-GIXD) and atomic force microscopy (AFM). The results show that the accelerating effect of the additive contributes to the self-aggregation of the converted molecules.

EXPERIMENTAL SECTION

Sample Preparation. A polycrystalline powder sample of PDK was synthesized according to previous studies.[12,13] Chloroform (Chl) and 1,2,4-trichlorobenzene (TCB) of ACS spectrophotometric grade were purchased from Sigma-Aldrich (Milwaukee, WI). The powder sample of PDK was dissolved in Chl at a concentration of 1.0 wt %. The solution was heated at approximately 353 K for 5 min to completely dissolve the solute, and the solution was then cooled

to room temperature. Meanwhile, another solution was prepared by adding TCB to the Chl solution in a 99:1 weight ratio.[14]

Film Preparation. An 8-inch silicon (Si) wafer with a thickness of 625 ± 25 μm manufactured by Valqua-FFT (Tokyo, Japan) was cut into rectangles with a size of 40 × 20 mm^2. The wafers were ultrasonically cleaned with ultrapure water, ethanol, acetone, and 1,2-dichloroethane sequentially for 1 minute each. The cleaned silicon substrates were further treated with ozone for 10 minutes on each side. Spin-coated films were prepared by dropping 20 μL of the PDK/Chl solution onto the cleaned wafers and spinning it at 2000 rpm for 1 minute using an Active (Saitama, Japan) ACT-300T spin coater. In this paper, films prepared from Chl solutions with and without TCB will be referred to as PDK/Chl and PDK/Chl-TCB films, respectively. The obtained film samples were photo-irradiated at a substrate temperature of 353 K, measured by a thermocouple mounted directly on the substrate surface. The photoconversion was performed for 1 hour in a nitrogen-filled environment using a LED lamp with a wavelength of 470 nm and an output of approximately 200 mW cm^{-2}. These are the optimal conditions for the photoconversion to the target material reported elsewhere.[14] The nominal thickness of the converted film was calculated to be about 25 nm by comparing its IR band intensity to that of a vapor-deposited film with a thickness of 50 nm.[25]

IR pMAIRS measurements. IR pMAIRS measurements were performed using a Thermo Fischer Scientific (Madison, WI, USA) Magna 550 Fourier transform IR (FT-IR) spectrometer equipped with a MAIRS automated analysis accessory (TN 10-1500). A germanium wire-grid linear polarizer (090-1500) purchased from PIKE Technologies (Madison, WI, USA) was used to generate p-polarized light. The aperture was set to the maximum of 150% (inner diameter of approximately 10 mm), and the wavenumber resolution was set to 4 cm^{-1}. The Blackman-Harris

function was employed for the apodization function through the IR measurements. The angle of incidence was set from 9 to 44° at 5° intervals, and transmitted light was detected with a mercury cadmium telluride (MCT) detector cooled with liquid nitrogen for at least 2 hours. The generated IP and OP spectra were converted to the corresponding OI spectrum by introducing the spectral intensities (A_{IP} and A_{OP}) into the following equation;[11]

$$A_{\mathrm{iso}} = \frac{1}{3}(2A_{\mathrm{IP}} + A_{\mathrm{OP}}), \quad (1)$$

where A_{iso} is the absorbance of the OI spectrum.

IR attenuated total reflection (ATR) measurements. IR ATR spectra were measured using a Magna 550 FT-IR spectrometer equipped with a Spectra-Tech (Oak Ridge, TN, USA) Foundation Thunder Dome ATR accessory without a polarizer. The attachment has a single-reflection IR element made of germanium with a fixed angle of incidence of 45°. An MCT detector cooled by liquid nitrogen was used to detect the reflected light. The aperture diameter was set to 34% (inner diameter of approximately 5 mm), and the wavenumber resolution was set to 4 cm^{-1} or 1 cm^{-1}. The band assignments were based on density functional theory (DFT) calculations using the Gaussian 16 software[24] with B3LYP/6-31G(d,p) as the base set. The calculated wavenumber was linearly scaled in accordance with previous reports.[17,25]

2D-GIXD measurements. 2D-GIXD measurements were performed using a Rigaku (Tokyo, Japan) SmartLab diffractometer equipped with a HyPix-3000 two-dimensional image detector. A sealed X-ray tube operating at 40 kV and 50 mA was used to generate Cu Kα radiation. The incident angle was fixed at 0.20°, and the exposure time for measuring diffraction images was 1800 seconds. The obtained images were corrected to a reciprocal-space map defined by the surface-parallel (q_{xy}) and perpendicular (q_z) components of the scattering vector using the SmartLab Studio II software.

AFM measurements. AFM measurements were performed using a Seiko Instruments (Chiba, Japan) NanoNavi IIs control station as the control device and a NanoCute scanning probe microscope unit as the observation device. Dynamic force mode was selected as the measurement mode, and a Si cantilever with a force contact of 19 N m^{-1} was used. The obtained AFM images were corrected for background distortion using the Gwyddion software.

RESULTS AND DISCUSSION

Spectral evidence of residual additives. As described in the introduction section, some additives promote the photoconversion reaction of PDK through the increase of the mobility of the precursor molecules in a thin film. For this purpose, good solvents for PDK with high-boiling points such as 1,2-dichlorobenzene and TCB are used as the additive.[14,15] Nevertheless, no evidence has been obtained so far that the additive molecules remain in the precursor film. In this study, the pMAIRS measurements are performed to identify the residual additive molecules.

The pMAIRS-OI spectra of the precursor films prepared from Chl solutions without and with TCB are shown in **Figure 2**a-i and ii, respectively. The band assignments are performed by comparing them to the simulated spectra obtained by the DFT calculations (**Figure 2**b-ii). For example, the two bands at 1750 cm^{-1} and 1734 cm^{-1} in **Figure 2**a correspond to the anti-symmetric and symmetric stretching vibrations of the carbonyl groups (ν(C=O)), while the CH out-of-plane deformation vibration (γ(CH)) of the fused ring shows a typical band at 749 cm^{-1}. Note that the spectra of the as-spun films roughly match that of a bulk PDK sample (**Figure 2**b-i), but some bands are shifted as typically found for the ν(C=O) and γ(CH) bands. These shifts should reflect differences in crystallinity, which will be discussed later.

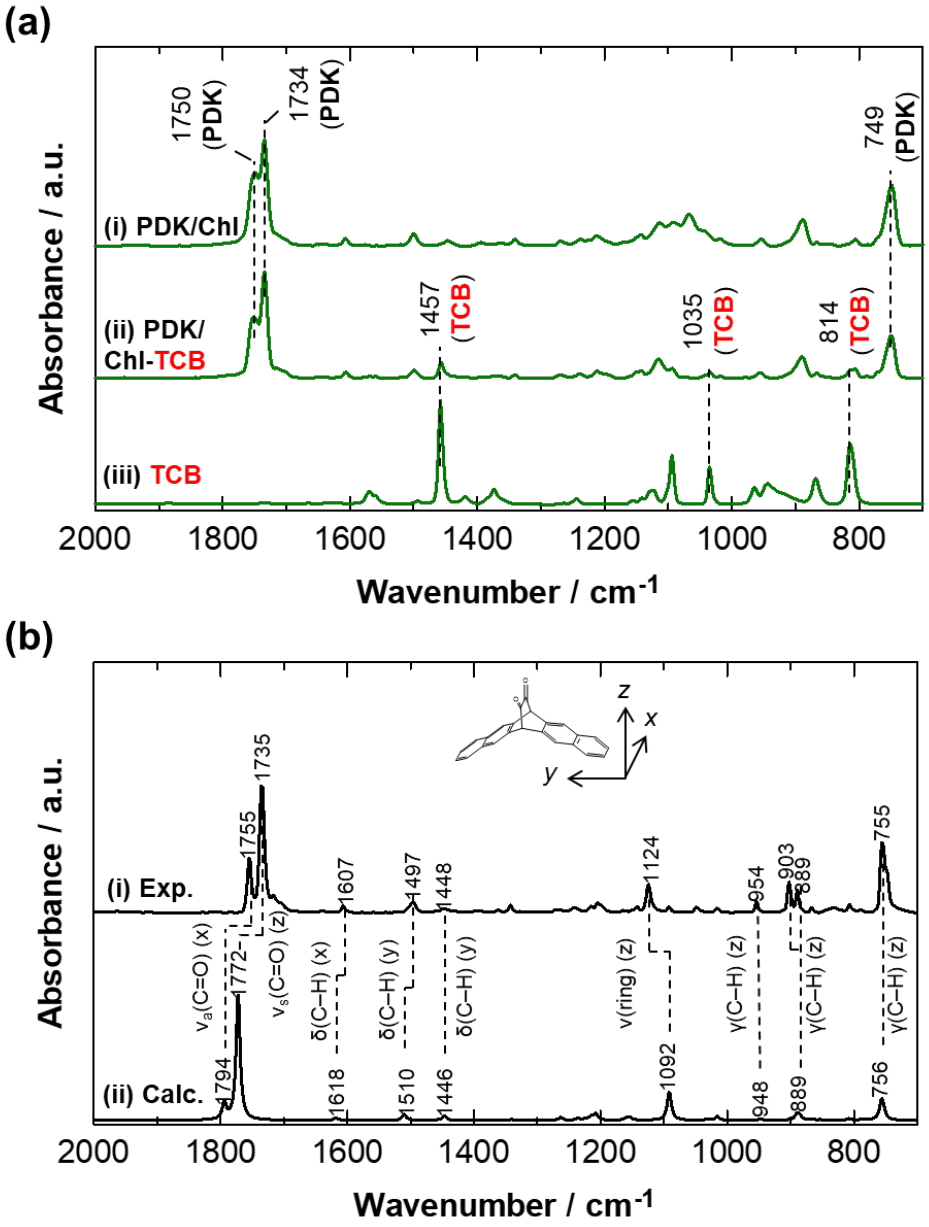

Figure 2. IR pMAIRS-OI spectra of spin-coated PDK films and ATR spectrum of pure TCB solvent (a). IR ATR spectrum of bulk PDK sample and simulated spectrum predicted by the DFT calculation (b).

For the precursor films, the two spectra in **Figure 2**a are basically similar to each other in terms of band positions and relative intensities, except for the band region of 1100–1050 cm^{-1} due to absorption of the oxide layer of the Si substrate.[26] Upon close inspection, however, some bands

appear to be unique to the spectrum of the PDK/Chl-TCB film, as found for the bands at 1457, 1035, and 814 cm^{-1}. These bands can easily be assigned to the vibrational modes of the solvent, TCB, by comparing the spectra (**Figure 2**a-ii and iii). This clearly indicates the presence of TCB still remained in the as-spun film, which has not been identified so far. Furthermore, the influence of residual TCB on the photoconversion from PDK to PEN is discussed below.

Quantitative analysis of photoconversion reactions. To discuss the structural conversion from PDK to PEN, we first examine the wavenumber region of 1800–1700 cm^{-1} in **Figure 2**a, in which the ν(C=O) bands of "PDK" are uniquely observed. After 1 hour of photoirradiation, the band intensity decreases dramatically for both PDK/Chl and PDK/Chl-TCB films as shown in **Figure 3**a. For the PDK/Chl-TCB film, in particular, the ν(C=O) bands of PDK almost disappear after the photoirradiation, whereas a weak but clear band remains in the spectrum of the photoconverted PDK/Chl film. Meanwhile, the γ(CH) band of "PEN"[27,28] appears at 906 cm^{-1} in the spectra (**Figure 3**b), indicating that the precursor compound reacts photochemically to produce the target material. This straightforwardly indicates that the conversion reaction quantitatively proceeds due to the accelerating effect of the additive. Note that the vibrational bands of TCB disappear after photoirradiation (Figure S1). This indicates that the residual additive is removed in the photoconverted film.

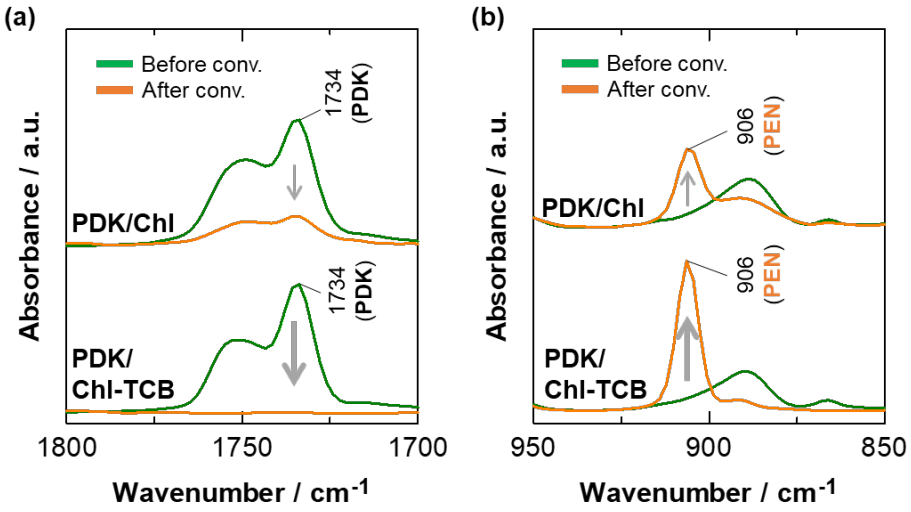

Figure 3. IR pMAIRS-OI spectra of photochemically converted PEN thin films in different wavenumber regions: 1800–1700 cm^{-1} (a) and 950–850 cm^{-1} (b).

An important advantage of using the pMAIRS technique is that the chemical reaction in the film can quantitatively be pursued for each chemical group by using the OI spectra. Assuming that sublimation and decomposition are negligible during the conversion reaction, the monitored rate of the decrease in the ν(C=O) band intensity of PDK should be consistent with the conversion rates before and after the photoirradiation. This assumption is reasonable considering that the substrate temperature during the photoirradiation is sufficiently low compared to the sublimation and decomposition temperature of PEN.[29] The analytical results of the pMAIRS-OI spectra show that the conversion rate of the PDK/Chl film is clearly lower than that of the PDK/Chl-TCB film (**Table 1**), which quantitatively confirms that the additive works out for accelerating the conversion reaction.

Table 1. Photoconversion rate of PDK estimated from pMAIRS spectra.

Precursor/Solvent	Conversion rate / %
PDK/Chl	87.6
PDK/Chl-TCB	~100

Influence on crystallinity and grain size. In the previous section, we discussed the influence of TCB on the conversion rate of PDK. In this section, the influences are investigated in terms of molecular aggregation in thin films. First, let us discuss the crystallographic properties on the basis of the 2D-GIXD patterns in **Figure 4**.

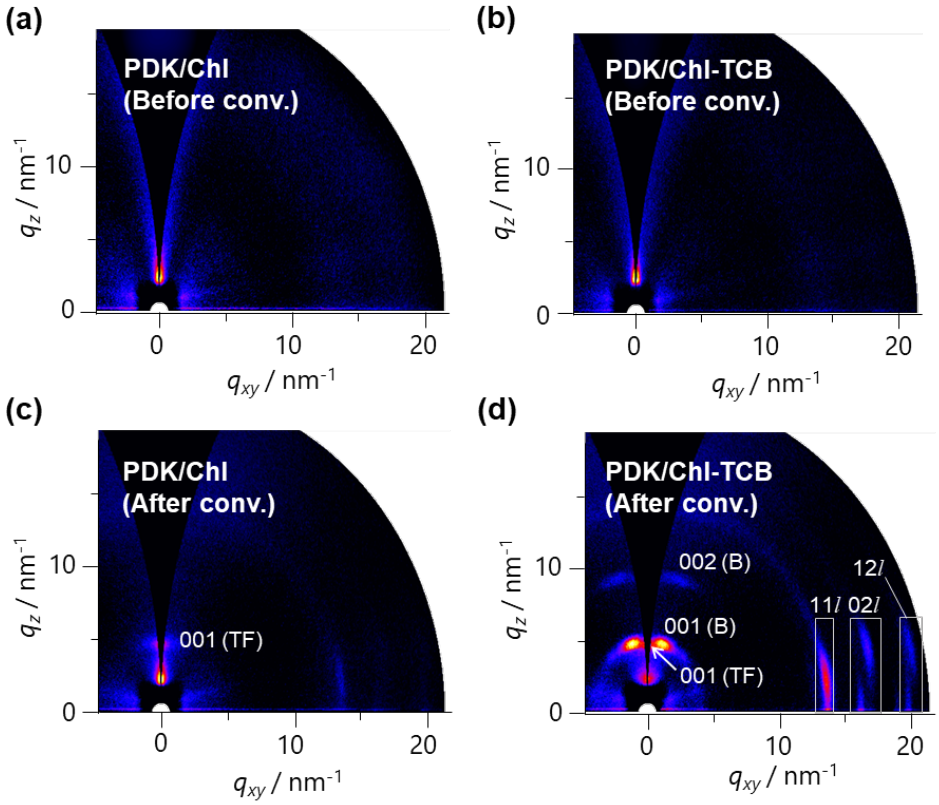

Figure 4. 2D-GIXD patterns of spin-coated PDK films (a, b) and photoconverted PEN films (c, d) prepared from Chl solutions with and without TCB. In (c) and (d), "TF" and "B" denote the thin-film and bulk phases of PEN, respectively.

No Bragg reflections are observed in the diffraction pattern of the as-spun films (**Figure 4**a, b), indicating that the precursor films have an amorphous structure for both solvents, which agrees with previous reports.[14,16] Since the precursor compound can form crystalline structures at room temperature,[12,19,20] this result implies that the amorphous structure in the spin-coated films is kinetically limited.[10,30,31] The amorphous structure is indeed confirmed by the featureless topographic images obtained from the AFM measurements in **Figure 5**a and b.

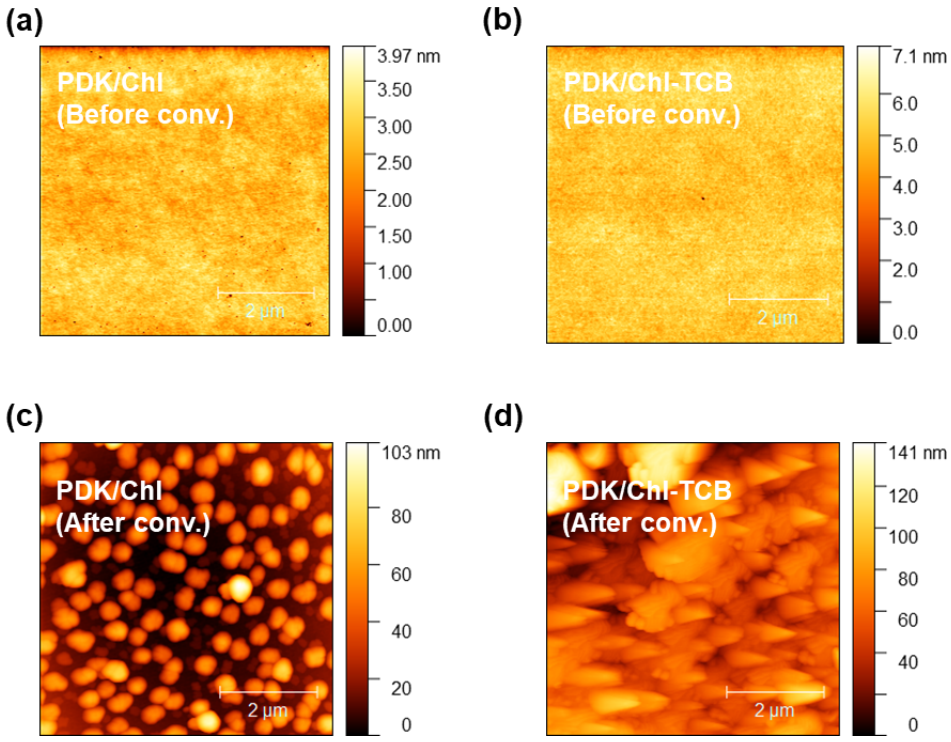

Figure 5. AFM topographic images of spin-coated PDK films (a, b) and photoconverted PEN films (c, d) prepared from Chl solutions with and without TCB.

After the photoconversion, diffraction spots commonly appear on the q_z axis for the PDK/Chl and PDK/Chl-TCB films as found in **Figure 4**c and d. The interlayer spacing calculated from the peak positions nearly corresponds to that of the (001) plane of the "thin-film phase" of PEN (1.54 nm).[32–34] Another polymorph, the "bulk phase",[35,36] is also generated in the PDK/Chl-TCB film as

evidenced by the peaks at a tilted position of about 10° from the q_z axis (**Figure 4**d). These characteristic peaks are typically observed for the bulk phase grown on the thin-film phase, and these are readily attributed to the 00*l* series reflections of the bulk phase by referring to literature.[37–39] It should be emphasized that the presence of the bulk phase in the photoconverted PEN films has been previously overlooked[14] and this is the first report.

The diffraction analysis shows that the thin-film and bulk phases coexist in the "photoconverted" film. This crystalline polymorphism is different from that of "thermally converted" PEN films, where the bulk phase is formed predominantly due to heat treatments at a high temperature.[10,11] This analysis suggests that in the case of photoconversion reactions, the use of relatively low temperatures during the photoconversion prevents a crystal transformation from the thin-film phase to the bulk phase. This is a practical advantage of using the photoconversion-type precursor when compared to thermally convertible precursors, since the thin-film phase is favorable for charge-transport in FETs.[40]

Comparing the diffraction patterns of the photoconverted films with and without TCB, the number of diffraction spots (or partial rings) is higher for the thin film having the additive (**Figure 4**d), indicating a highly crystalized structure of PEN. The additive-free thin film, in other words, has a less crystalline structure, which can also be understood from the relatively small grains in the AFM images shown in **Figure 5**c and d. It is also noteworthy that the diffraction peaks of the bulk phase are not clearly observed for the additive-free film (**Figure 4**c). This ambiguously weak intensity would suggest that the crystallites in the bulk phase are randomly oriented due to the low crystallinity. According to our previous studies on the precursor method for PEN,[10,11] unreacted precursor molecules disturb molecular aggregation of the product compound, resulting in a less

ordered film structure. Therefore, the low crystallinity of PEN in the photoconverted film without the additive would be due to the low conversion rate, as discussed earlier.

CONCLUSION

The pMAIRS technique has been applied to analyze the photoconversion reaction from PDK to PEN in spin-coated films, and the role of TCB used as an additive in the conversion reaction has been investigated. The spectral analysis demonstrates that the additive molecules remain in the film even after the evaporation of solvent used for spin coating, and that the residual additive completes the chemical reaction to produce the target material. This study emphasizes that the pMAIRS technique can be used to quantify chemical reactions in films. In this manner, this study provides not only insight into photoconversion chemistry, but also an analytical tool for quantitative analysis of on-surface reactions.

ASSOCIATED CONTENT

AUTHOR INFORMATION

Corresponding Author

*E-mail: nobutaka@env.kuicr.kyoto-u.ac.jp

ORCID

Nobutaka Shioya: 0000-0002-2915-894X

Hironobu Hayashi: 0000-0002-7872-3052

Hiroko Yamada: 0000-0002-2138-5902

Takeshi Hasegawa: 0000-0001-5574-9869

Notes

The authors declare no competing financial interests.

ACKNOWLEDGMENT

This work was financially supported by a Grant-in-Aid for Challenging Research (Exploratory) [21K18979 (T.H.)], a Grant-in-Aid for Scientific Research (B) [22H02106(T.H.)], a Grant-in-Aid for Early-Career Scientists [22K14604 (N.S.)] and a Grant-in-Aid for Transformative Research Areas "Dynamic Exciton" [JP20H05833 (H.Y.)] from the Japan Society for the Promotion of Science (JSPS), for which the authors are thankful. This work was partially supported by ISHIZUE 2023 of Kyoto University (H.Y.).

REFERENCES

1. Xie, P.; Liu, T.; Sun, J.; Yang, J. Structures, Properties, and Device Applications for [1]Benzothieno[3,2-b]Benzothiophene Derivatives. *Adv. Funct. Mater.* **2022**, *32* (21), 2200843. https://doi.org/10.1002/adfm.202200843.

2. Riera-Galindo, S.; Tamayo, A.; Mas-Torrent, M. Role of Polymorphism and Thin-Film Morphology in Organic Semiconductors Processed by Solution Shearing. *ACS Omega* **2018**, *3* (2), 2329–2339. https://doi.org/10.1021/acsomega.8b00043.

3. Iino, H.; Hanna, J. Liquid Crystalline Organic Semiconductors for Organic Transistor Applications. *Polym. J.* **2017**, *49* (1), 23–30. https://doi.org/10.1038/pj.2016.101.

4. Allard, S.; Forster, M.; Souharce, B.; Thiem, H.; Scherf, U. Organic Semiconductors for Solution-Processable Field-Effect Transistors (OFETs). *Angew. Chem. Int. Ed.* **2008**, *47* (22), 4070–4098. https://doi.org/10.1002/anie.200701920.

5. Yamada, H.; Kuzuhara, D.; Suzuki, M.; Hayashi, H.; Aratani, N. Synthesis and Morphological Control of Organic Semiconducting Materials Using the Precursor Approach. *Bull. Chem. Soc. Jpn.* **2020**, *93* (10), 1234–1267. https://doi.org/10.1246/bcsj.20200130.

6. Suzuki, M.; Aotake, T.; Yamaguchi, Y.; Noguchi, N.; Nakano, H.; Nakayama, K.; Yamada, H. Synthesis and Photoreactivity of α-Diketone-Type Precursors of Acenes and Their Use in Organic-Device Fabrication. *J. Photochem. Photobiol. C: Photochem. Rev.* **2014**, *18*, 50–70. https://doi.org/10.1016/j.jphotochemrev.2013.10.003.

7. Yamada, H.; Okujima, T.; Ono, N. Organic Semiconductors Based on Small Molecules with Thermally or Photochemically Removable Groups. *Chem. Commun.* **2008**, 26, 2957–2974. https://doi.org/10.1039/b719964c.

8. Afzali, A.; Dimitrakopoulos, C. D.; Graham, T. O. Photosensitive Pentacene Precursor: Synthesis, Photothermal Patterning, and Application in Thin-Film Transistors. *Adv. Mater.* **2003**, *15* (24), 2066–2069. https://doi.org/10.1002/adma.200305510.

9. Afzali, A.; Dimitrakopoulos, C. D.; Breen, T. L. High-Performance, Solution-Processed Organic Thin Film Transistors from a Novel Pentacene Precursor. *J. Am. Chem. Soc.* **2002**, *124* (30), 8812–8813. https://doi.org/10.1021/ja0266621.

10. Shioya, N.; Fujiwara, R.; Tomita, K.; Shimoaka, T.; Okudaira, K. K.; Yoshida, H.; Koganezawa, T.; Hasegawa, T. Monitoring of Crystallization Process in Solution-Processed Pentacene Thin Films by Chemical Conversion Reactions. *J. Phys. Chem. C* **2021**, *125* (4), 2437–2445. https://doi.org/10.1021/acs.jpcc.0c10431.

11. Shioya, N.; Fujiwara, R.; Tomita, K.; Shimoaka, T.; Hasegawa, T. Simultaneous Analysis of Molecular Orientation and Quantity Change of Constituents in a Thin Film Using pMAIRS. *J. Phys. Chem. A* **2020**, *124* (13), 2714–2720. https://doi.org/10.1021/acs.jpca.0c00111.

12. Yamada, H.; Yamashita, Y.; Kikuchi, M.; Watanabe, H.; Okujima, T.; Uno, H.; Ogawa, T.; Ohara, K.; Ono, N. Photochemical Synthesis of Pentacene and Its Derivatives. *Chem.—Eur. J.* **2005**, *11* (21), 6212–6220. https://doi.org/10.1002/chem.200500564.

13. Uno, H.; Yamashita, Y.; Kikuchi, M.; Watanabe, H.; Yamada, H.; Okujima, T.; Ogawa, T.; Ono, N. Photo Precursor for Pentacene. *Tetrahedron Lett.* **2005**, *46* (12), 1981–1983. https://doi.org/10.1016/j.tetlet.2005.01.157.

14. Nakayama, K.; Ohashi, C.; Oikawa, Y.; Motoyama, T.; Yamada, H. Characterization and Field-Effect Transistor Performance of Printed Pentacene Films Prepared by Photoconversion of a Soluble Precursor. *J. Mater. Chem. C* **2013**, *1* (39), 6244–6251. https://doi.org/10.1039/c3tc31083c.

15. Motoyama, T.; Kiyota, T.; Yamada, H.; Nakayama, K. Hetero-Layered Organic Photovoltaic Devices Fabricated Using Soluble Pentacene Photoprecursors. *Sol. Energy Mater. Sol. Cells* **2013**, *114*, 156–160. https://doi.org/10.1016/j.solmat.2013.02.023.

16. Masumoto, A.; Yamashita, Y.; Go, S.; Kikuchi, T.; Yamada, H.; Okujima, T.; Ono, N.; Uno, H. Organic Thin-Film Transistor from a Pentacene Photoprecursor. *Jpn. J. Appl. Phys.* **2009**, *48* (5R), 051505. https://doi.org/10.1143/jjap.48.051505.

17. Shioya, N.; Fujii, M.; Shimoaka, T.; Eda, K.; Hasegawa, T. Stereoisomer-Dependent Conversion of Dinaphthothienothiophene Precursor Films. *Sci. Rep.* **2022**, *12* (1), 4448. https://doi.org/10.1038/s41598-022-08505-5.

18. Hayashi, H.; Hieda, N.; Yamauchi, M.; Chan, Y. S.; Aratani, N.; Masuo, S.; Yamada, H. Visible-Light-Induced Heptacene Generation under Ambient Conditions: Utilization of Single-crystal Interior as an Isolated Reaction Site. *Chem.—Eur. J.* **2020**, *26* (66), 15079–15083. https://doi.org/10.1002/chem.202002155.

19. Yamauchi, M.; Miyamoto, Y.; Suzuki, M.; Yamada, H.; Masuo, S. Photoconversion of 6,13-α-Diketopentacene Single Crystals Exhibiting Light Intensity-Dependent Morphological Change. *Phys. Chem. Chem. Phys.* **2018**, *21* (12), 6348–6353. https://doi.org/10.1039/c8cp06594b.

20. Masuo, S.; Tanaka, K.; Oe, M.; Yamada, H. Photoconversion of 6,13-α-Diketopentacene in the Crystalline Phase. *Phys. Chem. Chem. Phys.* **2014**, *16* (26), 13483–13488. https://doi.org/10.1039/c4cp01607f.

21. Hasegawa, T.; Shioya, N. MAIRS: Innovation of Molecular Orientation Analysis in a Thin Film. *Bull. Chem. Soc. Jpn.* **2020**, *93* (9), 1127–1138. https://doi.org/10.1246/bcsj.20200139.

22. Hasegawa, T. Advanced Multiple-Angle Incidence Resolution Spectrometry for Thin-Layer Analysis on a Low-Refractive-Index Substrate. *Anal. Chem.* **2007**, *79* (12), 4385–4389. https://doi.org/10.1021/ac070676d.

23. Shimada, K.; Maruyama, S.; Miyadera, T.; Kaminaga, K.; Matsumoto, Y. Reaction Dynamics of $C(NH_2)_3SnI_3$ Formation from Vacuum-Deposited $C(NH_2)_3I$ and SnI_2 Bilayer Thin Films Investigated by In Situ Infrared Multiple-Angle Incidence-Resolved Spectroscopy. *ACS Appl. Mater. Interfaces* **2023**, *15* (38), 45411–45417. https://doi.org/10.1021/acsami.3c08708.

24. Frisch, M. J.; et al., *Gaussian 16, Revision C.01,* Gaussian, Inc., Wallingford CT, **2019**.

25. Yoshida, H.; Takeda, K.; Okamura, J.; Ehara, A.; Matsuura, H. A New Approach to Vibrational Analysis of Large Molecules by Density Functional Theory: Wavenumber-Linear Scaling Method†. *J. Phys. Chem. A* **2002**, *106* (14), 3580–3586. https://doi.org/10.1021/jp013084m.

26. Boyd, I. W. Deconvolution of the Infrared Absorption Peak of the Vibrational Stretching Mode of Silicon Dioxide: Evidence for Structural Order? *Appl. Phys. Lett.* **1987**, *51* (6), 418–420. https://doi.org/10.1063/1.98408.

27. Frątczak, E. Z.; Uznański, P.; Moneta, M. E. Characterization of Molecular Organization in Pentacene Thin Films on SiO2 Surface Using Infrared Spectroscopy, Spectroscopic Ellipsometry, and Atomic Force Microscopy. *Chem. Phys.* **2015**, *456*, 49–56. https://doi.org/10.1016/j.chemphys.2015.04.015.

28. Hosoi, Y.; Okamura, K.; Kimura, Y.; Ishii, H.; Niwano, M. Infrared Spectroscopy of Pentacene Thin Film on SiO_2 Surface. *Appl. Surf. Sci.* **2005**, *244* (1–4), 607–610. https://doi.org/10.1016/j.apsusc.2004.10.131.

29. Ye, X.; Liu, Y.; Han, Q.; Ge, C.; Cui, S.; Zhang, L.; Zheng, X.; Liu, G.; Liu, J.; Liu, D.; Tao, X. Microspacing In-Air Sublimation Growth of Organic Crystals. *Chem. Mater.* **2018**, *30* (2), 412–420. https://doi.org/10.1021/acs.chemmater.7b04170.

30. Tomita, K.; Shioya, N.; Shimoaka, T.; Okudaira, K. K.; Yoshida, H.; Koganezawa, T.; Hasegawa, T. Substrate-Independent Control of Polymorphs in Tetraphenylporphyrin Thin Films by Varying the Solvent Evaporation Time Using a Simple Spin-Coating Technique. *Cryst. Growth Des.* **2021**, *21* (9), 5116–5125. https://doi.org/10.1021/acs.cgd.1c00500.

31. Hada, M.; Shioya, N.; Shimoaka, T.; Eda, K.; Hada, M.; Hasegawa, T. Comprehensive Understanding of Structure-Controlling Factors of a Zinc Tetraphenylporphyrin Thin Film Using pMAIRS and GIXD Techniques. *Chem.—Eur. J.* **2016**, *22* (46), 16539–16546. https://doi.org/10.1002/chem.201603291.

32. Yoshida, H.; Inaba, K.; Sato, N. X-Ray Diffraction Reciprocal Space Mapping Study of the Thin Film Phase of Pentacene. *Appl. Phys. Lett.* **2007**, *90* (18), 181930. https://doi.org/10.1063/1.2736193.

33. Nabok, D.; Puschnig, P.; Ambrosch-Draxl, C.; Werzer, O.; Resel, R.; Smilgies, D.-M. Crystal and Electronic Structures of Pentacene Thin Films from Grazing-Incidence X-Ray Diffraction and First-Principles Calculations. *Phys. Rev. B* **2007**, *76* (23), 235322. https://doi.org/10.1103/physrevb.76.235322.

34. Schiefer, S.; Huth, M.; Dobrinevski, A.; Nickel, B. Determination of the Crystal Structure of Substrate-Induced Pentacene Polymorphs in Fiber Structured Thin Films. *J. Am. Chem. Soc.* **2007**, *129* (34), 10316–10317. https://doi.org/10.1021/ja0730516.

35. Siegrist, T.; Besnard, C.; Haas, S.; Schiltz, M.; Pattison, P.; Chernyshov, D.; Batlogg, B.; Kloc, C. A Polymorph Lost and Found: The High-Temperature Crystal Structure of Pentacene. *Adv. Mater.* **2007**, *19* (16), 2079–2082. https://doi.org/10.1002/adma.200602072.

36. Campbell, R. B.; Robertson, J. M.; Trotter, J. The Crystal Structure of Hexacene, and a Revision of the Crystallographic Data for Tetracene. *Acta Cryst.* **1962**, *15* (3), 289–290. https://doi.org/10.1107/s0365110x62000699.

37. Pachmajer, S.; Jones, A. O. F.; Truger, M.; Röthel, C.; Salzmann, I.; Werzer, O.; Resel, R. Self-Limited Growth in Pentacene Thin Films. *ACS Appl. Mater. Interfaces* **2017**, *9* (13), 11977–11984. https://doi.org/10.1021/acsami.6b15907.

38. Watanabe, T.; Hosokai, T.; Koganezawa, T.; Yoshimoto, N. In Situ Real-Time X-Ray Diffraction During Thin Film Growth of Pentacene. *Mol. Cryst. Liq. Cryst.* **2012**, *566* (1), 18–21. https://doi.org/10.1080/15421406.2012.701111.

39. Moser, A.; Flesch, H.-G.; Neuhold, A.; Marchl, M.; Ausserlechner, S. J.; Edler, M.; Griesser, T.; Haase, A.; Smilgies, D.-M.; Jakabovič, J.; Resel, R. Crystallization of Pentacene Thin Films on Polymeric Dielectrics. *Synth. Met.* **2012**, *161* (23–24), 2598–2602. https://doi.org/10.1016/j.synthmet.2011.09.027.

40. Chung, H.; Diao, Y. Polymorphism as an Emerging Design Strategy for High Performance Organic Electronics. *J Mater Chem C* **2016**, *4* (18), 3915–3933. https://doi.org/10.1039/c5tc04390e.